Green Chemistry

PAPER

View Article Online
View Journal

Cite this: DOI: 10.1039/d6gc01239f

Two-second surface-confined reconstruction of cellulose paper *via* a recyclable molten salt hydrate for water-resistant bioplastics

Ping Wang,†[a,b] Zhonglei Huang,†[b] Meiyan Wu,[b] Safoora Mirmohamadsadeghi,[c] Chao Liu,[b] Guang Yu,[b] Haishun Du,*[d] Jing Shen*[a,e] and Bin Li*[b]

The escalating plastic pollution crisis necessitates the development of sustainable bio-based materials with performance comparable to that of conventional plastics. Renewable and biodegradable cellulosic paper is an attractive alternative, yet its intrinsically poor water resistance and insufficient mechanical robustness limit its practical use. Conventional reinforcement strategies often rely on chemical modifiers, polymer coatings, or energy-intensive nanocellulose processing, increasing material complexity and environmental burden. Here, we report a 2-second surface-confined reconstruction strategy for cellulose paper using a recyclable molten salt hydrate ($LiBr{\cdot}3H_2O$) system. The treatment induces localized partial dissolution at the fibre surface without crystalline transformation or chemical derivatization, generating an interpenetrating nanofibril–microfibre network while preserving the bulk fibrous skeleton. The resulting cellulose-based bioplastic exhibits a dry tensile strength of 69.9 MPa and a wet tensile strength of 27.1 MPa, corresponding to 3.3-fold and 22.2-fold improvements compared to untreated cellulosic paper, respectively. The additive-free process avoids organic solvents and crosslinking agents while enabling solvent recovery, consistent with key principles of green chemistry. The demonstration of durable cellulose-based straws further confirms material performance under realistic service conditions. Life cycle assessment further demonstrates a reduced global warming potential compared with polyethylene and polylactic acid counterparts. This work establishes a solvent-efficient and scalable pathway for upgrading conventional cellulose materials into high-performance biodegradable plastic alternatives.

Received 28th February 2026,
Accepted 1st May 2026

DOI: 10.1039/d6gc01239f

rsc.li/greenchem

Green foundation

1. This work introduces an ultrafast solvent-mediated strategy using a recyclable molten salt hydrate to upgrade conventional cellulose paper into high-performance bioplastics without chemical derivatization or polymer additives. The surface-confined reconstruction minimizes material consumption and processing complexity while preserving the renewable cellulose framework.
2. The additive-free and short-duration treatment significantly reduces energy input and avoids the use of persistent synthetic polymers commonly required for paper reinforcement, enabling improved mechanical performance and water stability with a lower environmental footprint, as confirmed by life cycle assessment.
3. The proposed approach provides a scalable pathway for transforming abundant biomass-derived materials into durable and biodegradable plastic alternatives, supporting circular material utilization and advancing sustainable manufacturing toward reduced reliance on petroleum-based single-use plastics.

Introduction

Plastics have become indispensable in modern society due to their low cost, durability, and versatility. However, most commercial plastics are derived from petrochemical resources and exhibit extremely slow biodegradation in natural environments.[1–3] With only a small fraction of plastic waste being effectively recycled, the accumulation of persistent plastic debris has become a pressing global environmental challenge.[4] Developing sustainable, bio-based materials capable of partially replacing petroleum-derived plastics therefore represents an urgent and necessary strategy.[5–8] Cellulose,

[a]Research Division for Sustainable Papermaking & Advanced Materials, Key Laboratory of Biobased Materials Science and Technology of Ministry of Education, Northeast Forestry University, Harbin 150040, China. E-mail: Jing.Shen@unb.ca
[b]Qingdao New Energy Shandong Laboratory, System Integration Engineering Center, Qingdao Institute of Bioenergy and Bioprocess Technology, Chinese Academy of Sciences, Qingdao 266101, China. E-mail: libin@qibebt.ac.cn
[c]Department of Biotechnology, Faculty of Biological Science and Technology, University of Isfahan, Isfahan 81746-73441, Iran
[d]Department of Forestry, Michigan State University, East Lansing, 48824, USA. E-mail: hdu@msu.edu
[e]Limerick Pulp and Paper Centre, Department of Chemical Engineering, University of New Brunswick, Fredericton, NB E3B 6C2, Canada. E-mail: Jing.Shen@unb.ca
†These authors contributed equally.

the most abundant renewable polymer on Earth, is biodegradable, cost-effective, and readily available at a large scale.[9,10] Cellulosic paper has thus emerged as a promising candidate for biodegradable plastic alternatives.[11–14] High mechanical strength and water resistance are essential for practical paper-based plastic substitutes.[15] Recent perspectives on bioplastics have emphasized that sustainable alternatives to conventional plastics must meet not only criteria of renewability and biodegradability, but also deliver balanced engineering performance, scalable processing, and practical end-of-life compatibility.[16,17] In this context, mechanical robustness, water resistance, barrier performance, manufacturability, and environmental compatibility are increasingly recognized as key benchmarks for next-generation bioplastic materials. Nevertheless, the intrinsic hydrophilicity of cellulose, coupled with its limited mechanical robustness, continues to constrain its broader application, particularly under humid or aqueous conditions.[18,19]

Various strategies have been developed to improve the mechanical performance and water resistance of cellulose paper, including surface sizing,[20,21] chemical crosslinking,[18,22] nanocellulose reinforcement,[23,24] and solvent treatment.[25] Among these approaches, nanocellulose has attracted considerable attention and has been widely employed to enhance the mechanical properties of cellulose paper owing to its outstanding intrinsic strength and renewable origin.[26] Common reinforcement strategies include wet blending with pulp fibres, surface coating, and layer-by-layer assembly. For instance, Wang *et al.*[5] hybridized cellulose nanofibres with micro-scale cellulose fibres to fabricate fully biodegradable straws with tensile strengths of approximately 70 MPa, surpassing most commercial plastic straws. However, the intrinsic hydrophilicity of nanocellulose, arising from its abundant hydroxyl groups, substantially reduced wet mechanical strength (≈13 MPa), limiting performance under humid conditions. To address compatibility and water resistance, multilayer and composite coating strategies have been explored. Silva *et al.*[27] constructed alternating trilayer and pentalayer architectures based on electrostatic interactions between negatively charged natural rubber latex and positively charged cellulose nanofibres, improving interfacial adhesion and overall performance. Similarly, Shankar *et al.*[28] prepared styrene-acrylic copolymer/CNF nanocomposite emulsions and applied them as coatings to kraft paper, achieving enhanced mechanical strength and water resistance. Kwak *et al.*[29] coated paper straws with poly (butylene succinate)/cellulose nanocrystal (PBS/CNC) composites, where CNCs enhanced adhesion to the paper substrate and reinforced the polyester coating, thereby imparting improved water resistance, anti-fizzing behavior, and mechanical durability to the straws. Despite these advances, most nanocellulose-based reinforcement strategies rely on the external addition of nanofibrils and often involve multiple processing steps, interfacial engineering, or polymeric modifiers.[30] The production of nanocellulose itself typically requires high energy input, and aggregation during processing can compromise reinforcement efficiency. More importantly, the reliance on added components increases material complexity and processing burden, thereby limiting sustainability and large-scale applicability. These limitations suggest that directly reconstructing the internal structure of cellulose paper, rather than introducing external reinforcing phases, may offer a more efficient and sustainable pathway to achieve simultaneous mechanical strengthening and water stability.

Molten salt hydrates (MSHs) are a class of inorganic ionic liquid-like solvent systems in which water molecules coordinate metal cations at near-saturation ratios. Owing to their negligible vapor pressure, relatively low viscosity, thermal stability, and potential recyclability, MSHs have emerged as effective solvents for cellulose processing.[31] In particular, systems such as $LiBr{\cdot}3H_2O$ (LBTH) and $AlCl_3/ZnCl_2{\cdot}4H_2O$ have been shown to disrupt cellulose hydrogen bonding and activate crystalline domains under controlled conditions.[32–34] These characteristics suggest that a carefully regulated MSH treatment could induce surface-confined partial dissolution of cellulose fibres, rather than complete bulk dissolution. Such localized activation may enable the *in situ* generation of reinforcing nanofibrils while preserving the micro-scale fibrous framework, thereby reconstructing the internal architecture of cellulose paper without chemical derivatization. This structural reorganization is expected to densify the inter-fibre network and enhance mechanical integrity. Importantly, the ability to recover and reuse LBTH provides a basis for closed-loop processing, supporting a solvent-efficient and sustainable manufacturing pathway.[32] However, the feasibility of employing LBTH to achieve controlled surface-confined reconstruction of cellulose paper, without additional solvents, coatings, or crosslinking agents, remains underexplored. Moreover, the reinforcement mechanism associated with surface nanofibrillation, particularly the filling of inter-fibre voids and the formation of a densified interpenetrating network, has not yet been systematically elucidated.

Building on this rationale, we developed a 2-second LBTH pretreatment at 120 °C to fabricate water-resistant cellulose-based bioplastics through surface-confined structural reconstruction. During this ultrashort activation, the micro-scale cellulose skeleton is retained, while localized partial dissolution at the fibre surface generates *in situ* nanofibrils that fill inter-fibre voids and densify the network. The resulting interpenetrating nanofibril–microfibre architecture enhances load transfer within the fibrous matrix and improves resistance to water-induced weakening. The optimized bioplastic exhibits a dry tensile strength of 69.9 MPa and a wet tensile strength of 27.1 MPa, corresponding to 3.3-fold and 22.2-fold increases relative to untreated cellulose paper, respectively. After one week of water immersion, the bioplastic maintains structural integrity and sustains a 10 kg load (Fig. 1b and Video S1). Furthermore, a comprehensive comparison of mechanical performance, thermal stability, degradability, manufacturability, and green synthesis with representative commercial plastics and biomass-based plastics demonstrates the superior overall performance of the cellulose bioplastic (Fig. 1c).[35–38] In addition to its outstanding strength, the material also exhibits excellent solvent resistance and biodegradability. Collectively,

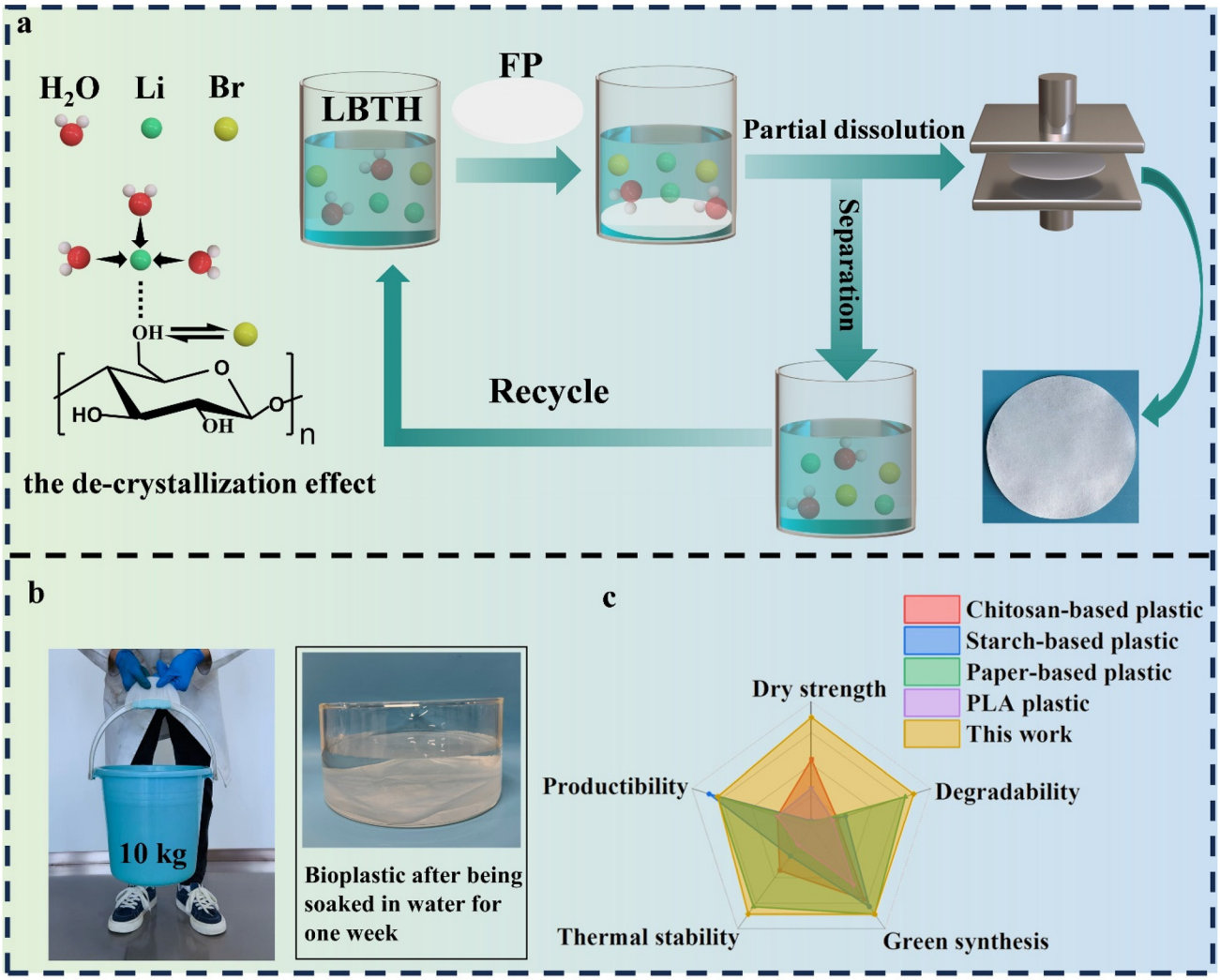

Fig. 1 Schematic illustration of the preparation of cellulose-based bioplastics. (a) Schematic illustration for preparing cellulose-based bioplastics. (b) Mechanical performance of the optimized cellulose-based bioplastic under wet conditions. (c) Radar chart comparing the comprehensive performance of chitosan-based plastics, starch-based plastics, paper-based bioplastics, polylactic acid (PLA) plastics, and the cellulose-based bioplastics developed in this work.

this strategy provides an additive-free and solvent-efficient pathway for upgrading cellulose paper toward sustainable plastic alternatives.

Results and discussion

Fabrication of cellulose-based bioplastics

As illustrated in Fig. 1a, cellulose paper (filter paper (FP)) is immersed in a preheated aqueous LBTH solution, followed by thorough washing with deionized water to remove residual salts. The treated material was subsequently hot-pressed to obtain a smooth and densified bioplastic. The dissolution behavior of cellulose in MSHs, such as LBTH, differs fundamentally from that in conventional cellulose solvent systems, such as ionic liquids and *N*-methylmorpholine *N*-oxide (NMMO).[39–41] In MSH systems, cellulose dissolution involves progressive disruption of hydrogen bonding, defibrillation, and structural deconstruction and may be accompanied by partial depolymerization under elevated temperatures.[40] In LBTH, lithium ions coordinate with oxygen atoms of cellulose hydroxyl groups, while bromide ions interact with hydroxyl protons, collectively weakening intra- and intermolecular hydrogen bonding.[42–45] At temperatures above 100 °C, proton-assisted cleavage of glycosidic bonds can occur, leading to a reduced degree of polymerization. Therefore, temperature and exposure time critically govern the balance between structural activation and cellulose degradation.[43,46] Given the strong sensitivity of LBTH–cellulose interactions to processing conditions, variations in treatment temperature and immersion time are expected to induce distinct structural evolutions within the fibrous network, ranging from fibre swelling and

surface activation to partial depolymerization. To achieve controlled surface nanofibrillation while preserving the original micro-scale skeleton, the effects of LBTH temperature and immersion time on both dry and wet tensile properties of the resultant bioplastics were systematically investigated.

Representative stress–strain curves under dry and wet conditions are presented in Fig. 2a–f. At 100 °C, extending the immersion time from 2 s to 10 s progressively enhanced the dry tensile strength of the modified filter paper (MFP) (Fig. 2a and Fig. S1a), indicating that moderate swelling and surface loosening improved inter-fibre contact and load transfer. However, further increasing the treatment time to 20 s led to slight reductions in both tensile strength and elongation at break, suggesting that prolonged exposure weakened the fibre network without providing additional reinforcement. A similar time-dependent trend was observed at 110 °C (Fig. 2b and Fig. S1b), although the overall strength enhancement was more pronounced. The sample treated for 6 s (MFP_{110}-6) reached a maximum dry tensile strength of 61.9 MPa, while longer immersion times resulted in gradual deterioration, consistent with partial damage to the micrometer-scale fibre skeleton due to excessive dissolution. At 120 °C, the sensitivity of dry tensile performance to immersion time became more significant (Fig. 2c and Fig. S1c). Among all tested conditions, MFP_{120}-2 exhibited the highest dry tensile strength (69.9 MPa), corresponding to an approximately 3.3-fold increase relative to untreated FP. Immersion times beyond 2 s caused a monotonic decline in strength, indicating that ultrashort exposure at elevated temperatures is essential for achieving controlled surface activation while preserving structural integrity. To

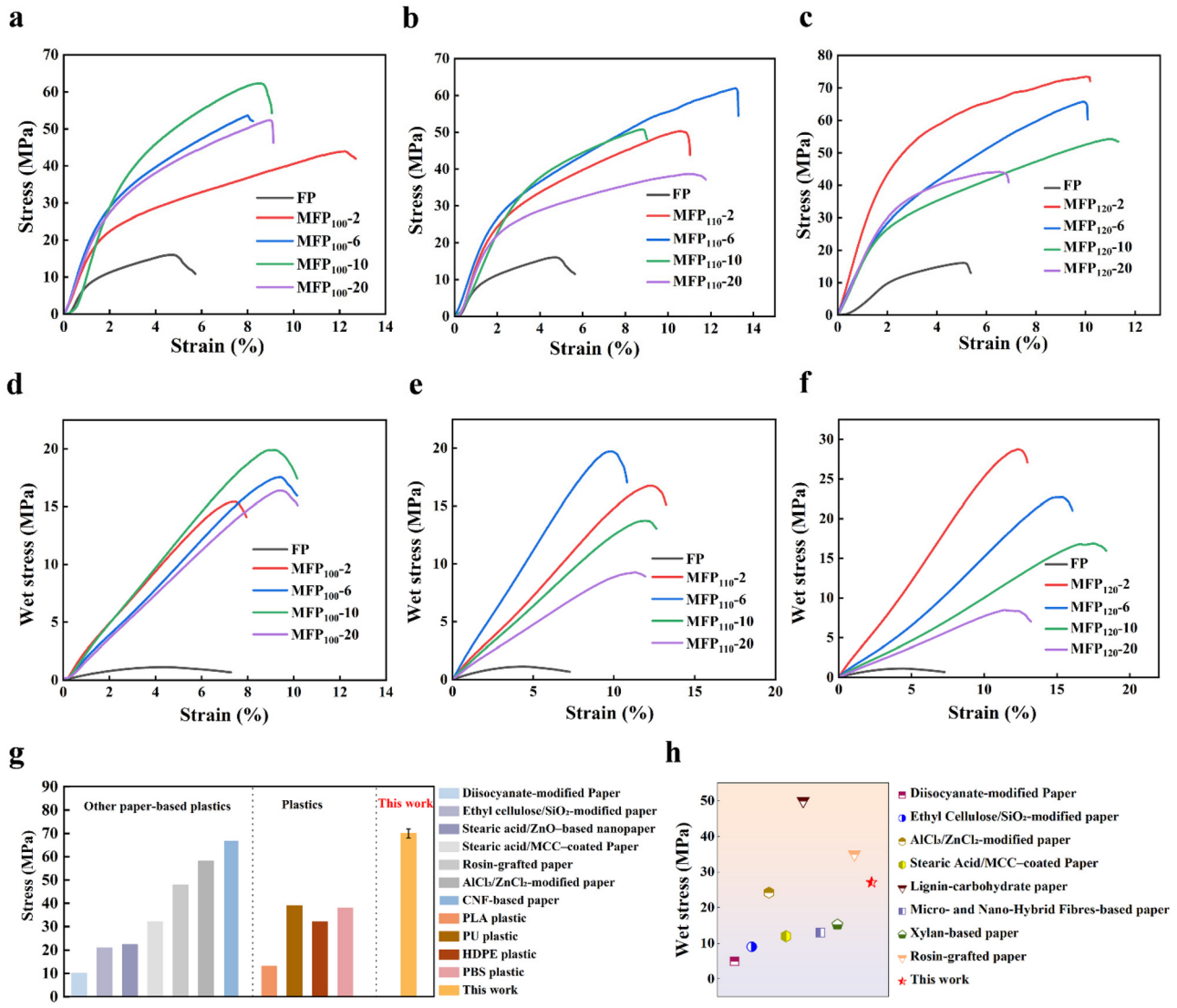

Fig. 2 Mechanical performance of the cellulose-based bioplastics. (a–c) Dry tensile stress–strain curves of cellulose-based bioplastics obtained after LBTH treatment at 100 °C (a), 110 °C (b), and 120 °C (c) for different immersion durations. (d–f) Corresponding wet tensile stress–strain curves recorded after water immersion for 24 h. (g) Comparison of the dry tensile strength of MFP_{120}-2 with that of previously reported plastic materials. (h) Comparison of the wet tensile strength of MFP_{120}-2 with that of reported cellulose paper-based plastics.

further elucidate the effect of temperature, samples treated for 2 s at 100–140 °C were compared (Fig. S2a and b). The dry tensile strength increased steadily from 100 °C to 120 °C and then decreased at 130 °C and 140 °C. This non-monotonic dependence confirms that 120 °C provides an optimal balance between surface-confined partial dissolution and network preservation. At higher temperatures, over-dissolution likely disrupts load-bearing fibre continuity, leading to reduced mechanical performance.

The wet-state tensile properties follow trends similar to those observed under dry conditions but exhibit substantially greater contrast relative to FP (Fig. 2d–f). The untreated FP displays an extremely low wet tensile strength (<2 MPa), reflecting the susceptibility of its loose bonded fibrous network to water-induced weakening. At 100 °C, the wet tensile strength increases with immersion time, reaching approximately 20 MPa at 10 s before slightly declining at 20 s (Fig. 2d and Fig. S1d). A comparable time-dependent behavior is observed at 110 °C, where MFP_{110}-6 achieves the highest wet strength at this temperature (19.7 MPa) (Fig. 2e and Fig. S1e). More pronounced improvements are obtained at 120 °C (Fig. 2f and Fig. S1f). Among all tested conditions, MFP_{120}-2 exhibits a wet tensile strength of 27.1 MPa, corresponding to a 22.2-fold increase relative to the untreated FP. Prolonged immersion beyond 2 s leads to reduced wet strength, consistent with partial disruption of the load-bearing fibre framework due to over-dissolution. When the immersion time is fixed at 2 s and the temperature varies from 100 to 140 °C, the wet tensile strength exhibits a non-monotonic dependence similar to that observed under dry conditions, increasing steadily from 100 °C to 120 °C and decreasing at 130 °C and 140 °C (Fig. S2c and d). The simultaneous enhancement of both dry and wet tensile properties indicates that short-duration treatment (*e.g.*, 2 s) at 120 °C achieves an optimal balance between surface activation and structural preservation. This behavior is attributed to the formation of a densified interpenetrating nanofibril–microfibre network at the fibre surface, which reinforces inter-fibre bonding and effectively suppresses fibre slippage and debonding in aqueous environments.

As shown in Fig. 2g and h, the dry and wet tensile strengths of MFP_{120}-2 are comparable to or exceed those of representative commercial plastics and most reported paper-based bioplastics.[5,13,18,35–37,47–55] These results demonstrate the potential of the reconstructed cellulose network as a mechanically robust and water-resistant alternative to conventional petroleum-derived plastics.

Theoretical analysis of the partial dissolution strategy

To elucidate the influence of LBTH treatment temperature and immersion time on the structural evolution of FP, the crystallinity index (CrI) was calculated from the XRD patterns (Fig. 3a–c). The CrI reflects the relative fraction of crystalline regions in cellulose and is closely associated with the integrity of the load-bearing fibrous network skeleton.[56] All treated samples retain the characteristic diffraction peaks of cellulose Iβ at $2\theta \approx 14.8°$ ((1–10)), 16.4° ((110)), 22.6° ((200)), and 34.5° ((004)), indicating the preservation of the native crystalline allomorph after LBTH treatment.[57] No peaks corresponding to cellulose II are detected, suggesting that the process induces structural activation rather than crystalline phase transformation. As shown in Fig. 3a and b, the CrI decreases progressively with increasing immersion time, consistent with partial disruption of hydrogen bonding within amorphous regions as well as at crystalline–amorphous interfaces and swelling of cellulose fibres.[42] At relatively short treatment time, the limited reduction in crystallinity indicates insufficient structural activation to promote extensive surface reconstruction, which correlates with the presence of loosely exposed micrometer-scale fibres (Fig. S3a and b). In contrast, prolonged treatment results in a more pronounced decrease in CrI, implying excessive disruption of crystalline domains and partial loss of fibrous integrity. Correspondingly, smoother and less defined surface morphologies are observed (Fig. S3c and d), which are unfavorable for effective load transfer.

At 120 °C (Fig. 3c), the cellulose paper treated for 2 s (MFP_{120}-2) exhibits a noticeable but controlled reduction in CrI relative to the FP. Elevated temperatures enhance ion cellulose interactions, promoting localized disruption of crystalline–amorphous interfaces while preserving the bulk fibre framework. This moderate structural activation is consistent with the formation of a densified interpenetrating nanofibril–microfibre network (Fig. 4b). In contrast, further extending the immersion time to 20 s leads to further reduction in CrI, indicative of over-dissolution and partial collapse of the original fibrous skeleton. These structural trends align with the non-monotonic mechanical performance observed under the corresponding treatment conditions.

The surface chemical properties of FP and treated samples were examined by Fourier transform infrared spectroscopy (FTIR), as shown in Fig. 3d. Because LBTH was used as the processing medium without chemical derivatization, no additional functional groups were anticipated. The FTIR spectrum of FP exhibits characteristic absorption bands at approximately 2886 cm^{-1} (C–H stretching) and 1640 cm^{-1} (O–H bending associated with absorbed water).[58] A broad band centered around 3381 cm^{-1} corresponds to O–H stretching vibrations arising from intermolecular hydrogen bonding and interactions with bound water. After LBTH treatment, the O–H stretching band of MFP_{120}-2 shifts to a lower wavenumber (3293 cm^{-1}), indicating strengthened hydrogen bonding interactions within the reconstructed cellulose network.[59,60] Deconvolution analysis of the 3000–3700 cm^{-1} region further reveals that the hydrogen-bonding fraction in MFP_{120}-2 (58.3%) is higher than that of FP (48.4%) (Fig. 3e and f). This enhancement can be attributed to the *in situ* generated nanofibrils that bridge adjacent microfibres (Fig. 4), promoting the formation of additional interfacial hydrogen bonds. Such reinforced intermolecular interactions correlate with the observed improvement in tensile performance.

X-ray photoelectron spectroscopy (XPS) further confirms the preservation of the cellulose chemical structure after LBTH treatment. Both FP and MFP_{120}-2 display three characteristic C

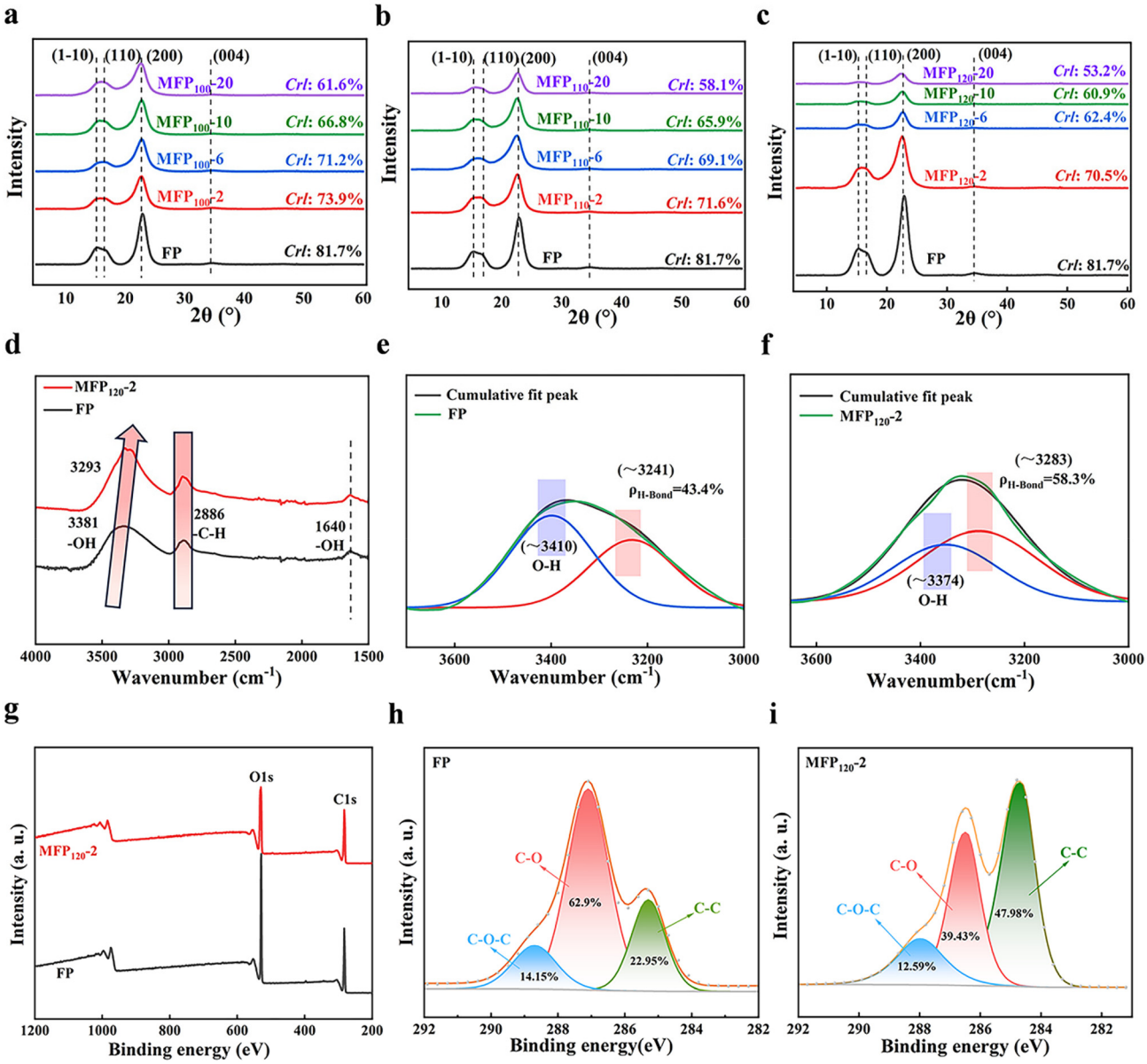

Fig. 3 Chemical and structural characterization of FP and MFP samples. (a–c) XRD patterns and corresponding crystallinity index (CrI) values of cellulose-based bioplastics obtained after LBTH treatment at 100 °C (a), 110 °C (b), and 120 °C (c) for different immersion durations. (d) FTIR spectra of FP and MFP_{120}-2. (e and f) Deconvolution and peak fitting of the FTIR spectra of FP (e) and MFP_{120}-2 (f). (g) XPS survey spectra of FP and MFP_{120}-2. (h and i) High-resolution C 1s XPS spectra of FP (h) and MFP_{120}-2 (i).

1s peaks at 284.8 eV (C–C), 286.3 eV (C–O), and 287.8 eV (C–O–C), in agreement with literature reports.[61] No new peaks or significant binding energy shifts are observed in either the C 1s or O 1s regions, indicating that no chemical derivatization occurs during processing. A slight decrease in the relative proportion of C–O–C components (from 14.15% in FP to 12.59% in MFP_{120}-2) is observed, which may reflect localized structural rearrangement associated with partial dissolution and reorganization at the fibre surface.[62] Importantly, the absence of new functional groups and major spectral shifts supports that the treatment primarily induces physical reconstruction rather than chemical derivatization.

The microstructure of paper-based materials is closely associated with their mechanical performance. Scanning electron microscopy (SEM) images (Fig. 4a and b) provide direct evidence of structural evolution after LBTH treatment. As shown in Fig. 4a, FP consists of loosely entangled cellulose fibres forming a porous network. The fibre surfaces appear rough, and abundant inter-fibre voids are observed, indicating limited contact area and weak interfacial bonding. After treatment at 120 °C for 2 s, MFP_{120}-2 exhibits a markedly densified surface morphology (Fig. 4b). High-magnification images reveal a compact interpenetrating structure in which nanoscale fibrillar features are distributed among the original microfi-

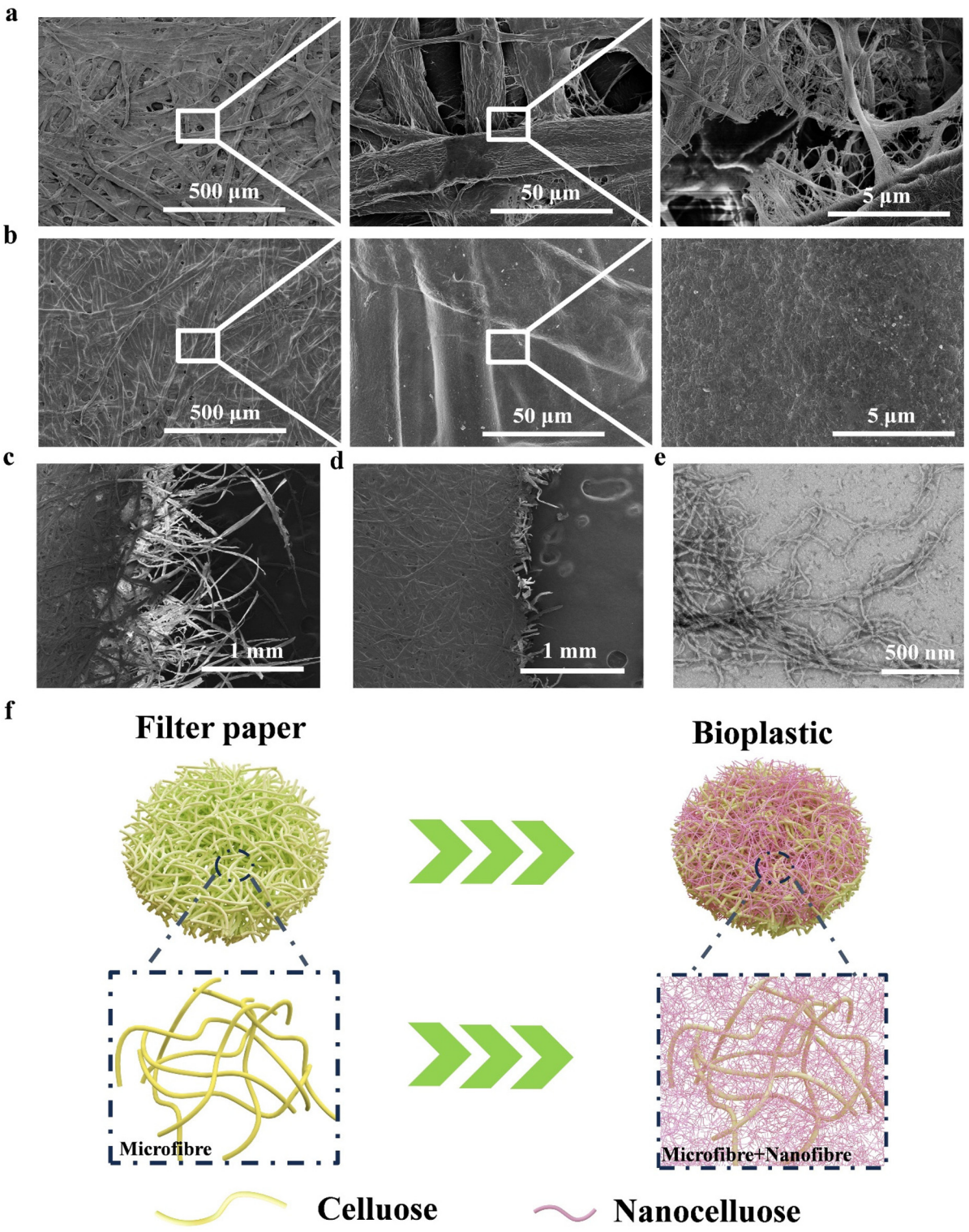

Fig. 4 Microstructural characterization of FP and MFP_{120}-2. (a and b) SEM images of FP (a) and MFP_{120}-2 (b). (c and d) SEM images of the fracture surfaces of FP (c) and MFP_{120}-2 (d) after tensile testing. (e) TEM image of nanofibrils scraped from the surface layers of MFP_{120}-2. (f) Schematic illustration of the structural evolution of cellulose paper during LBTH treatment.

bres. This morphology is consistent with surface-confined partial dissolution of cellulose, followed by localized regeneration and reorganization at the fibre interfaces, while the overall micrometer-scale fibrous framework remains intact. The resulting nanofibril–microfibre interpenetrating network increases inter-fibre contact area and promotes more effective

load transfer, leading to significant improvement in the mechanical performance and wet stability. To further substantiate this densification beyond qualitative SEM observations, the density of the samples was quantitatively analyzed.[63] The density of FP and MFP_{120}-2 was determined based on mass and geometrical volume measurements. The bulk density increased from 0.48 g cm^{-3} for FP to 0.71 g cm^{-3} for MFP_{120}-2, indicating a substantial reduction in the void volume within the fibrous network (Fig. S4).

The fracture morphologies after uniaxial tensile testing further support this structural interpretation. As shown in Fig. 4d, FP exhibits a highly disordered fracture surface characterized by evident fibre pull-out and slippage. In contrast, MFP_{120}-2 exhibits a comparatively compact and cohesive fracture surface (Fig. 4c), suggesting restricted fibre mobility and enhanced inter-fibre bonding.[47] The suppression of microfibre slippage is consistent with the improved tensile performance observed in both dry and wet states.

Transmission electron microscopy (TEM) analysis of surface layers scraped from LBTH-treated FP reveals fibrillar structures with diameters of tens of nanometers (Fig. 4e). These observations further support the formation of nanoscale cellulose fibrils at the treated fibre surface. As schematically illustrated in Fig. 4f, LBTH treatment induces controlled surface activation, generating nanoscale fibrils that bridge adjacent microfibres and densify the fibrous network without collapsing the bulk skeleton. This hierarchical structural reconstruction underpins the enhanced mechanical strength and wet stability of MFP_{120}-2. Unless otherwise specified, MFP_{120}-2 was selected for subsequent characterization.

Other properties of cellulose-based bioplastics

Conventional plastic materials often exhibit limited dimensional stability at elevated temperatures due to thermal softening or expansion.[64,65] In contrast, the reconstructed cellulose-based bioplastic inherits the intrinsic thermal robustness of the cellulose fibres while benefiting from structural densification induced by LBTH treatment. Coefficient of thermal expansion (CTE) measurements (Fig. 5a) show that the MFP_{120}-2 bioplastic exhibits a remarkably low and negative CTE value of −69.89 μm m^{-1} $°C^{-1}$ over the temperature range of 0–120 °C. This negative thermal expansion behavior is attributed to the constrained hierarchical nanofibril–microfibre interpenetrating network, in which inter-fibre bonding restricts thermally induced dimensional changes.[66,67] By comparison, commonly used commercial plastics such as polypropylene (PP), polyethylene (PE), polyurethane (PU), and polylactic acid (PLA) display substantially higher positive CTE values within the same temperature range. Consistent with these quantitative results, noticeable softening and shrinkage are observed for commercial plastics after heating at 120 °C for 5 min, whereas the MFP_{120}-2 bioplastic maintains its structural integrity without discernible deformation (Fig. 5b). In addition to dimensional stability under practical service conditions, the cellulose-based bioplastic avoids thermoplastic flow and potential release of plastic-derived microfragments, which is advantageous for beverage-contact applications. Thermogravimetric analysis (TGA) further demonstrates that MFP_{120}-2 retains high thermal stability, exhibiting a maximum weight-loss temperature of 348 °C, only slightly lower than that of pristine cellulose paper (358 °C) (Fig. S5).[68] These results suggest that the LBTH treatment preserves the intrinsic thermal resistance of cellulose while enabling structural reinforcement.

The intrinsic hydrophilicity of cellulose generally results in limited water resistance in paper-based materials, restricting their practical use in humid or aqueous environments.[69,70] To evaluate water stability, FP and MFP_{120}-2 were immersed in water for 7 days and their water uptake behaviors were examined. As shown in Fig. 5c, FP exhibits a water uptake of 135%, whereas MFP_{120}-2 shows a significantly reduced water uptake of 82%, indicating improved resistance to water penetration following LBTH treatment. Notably, after prolonged water immersion, MFP_{120}-2 retains a wet tensile strength of approximately 25 MPa. A MFP_{120}-2 strip with a thickness of 0.1 mm and a width of 20 mm is capable of supporting a 1000 g load without noticeable deformation (Fig. 5d), demonstrating maintained mechanical integrity under aqueous conditions. In addition, MFP_{120}-2 exhibits a relatively low oxygen transmission rate (OTR), as shown in Fig. S6, suggesting improved barrier performance relevant to packaging applications. The enhanced wet stability of MFP_{120}-2 can be attributed not only to the reduced water uptake, but also to the reconstruction of interfibre interactions and the increased compactness of the fibrous network. In FP, the fibre network is primarily maintained by conventional hydrogen bonding and physical entanglement. Upon water immersion, water molecules readily penetrate the interfibre regions, weaken hydrogen-bonding interactions, and promote fibre swelling and slippage, leading to rapid deterioration of the mechanical integrity. In contrast, the ultrafast LBTH treatment induces a surface-confined reconstruction of cellulose fibres, generating nanofibrillar features and increasing the effective contact area between adjacent fibres. After washing and hot pressing, these reconstructed surface regions facilitate stronger interfibre bonding, while the nanofibrillar material serves as a bridging phase between neighbouring microfibres. As a result, a more compact and interconnected nanofibril–microfibre network is formed, reducing open voids and limiting water-accessible pathways within the paper structure. Such structural reorganization suppresses fibre swelling, slippage, and debonding in the wet state, thereby enabling the treated paper to retain high strength even after prolonged water exposure.

The solvent resistance of MFP_{120}-2 was further evaluated by immersion in representative organic solvents, including ethanol, isopropanol, acetone, tetrahydrofuran, and dimethylformamide (Fig. 5e). After 7 days of exposure, no apparent discoloration or dimensional deformation is observed (Fig. S7a). Mechanical testing further shows that tensile strengths remain within 18–26 MPa after solvent immersion (Fig. S7b and c), indicating preservation of structural integrity. These results suggest that the reconstructed

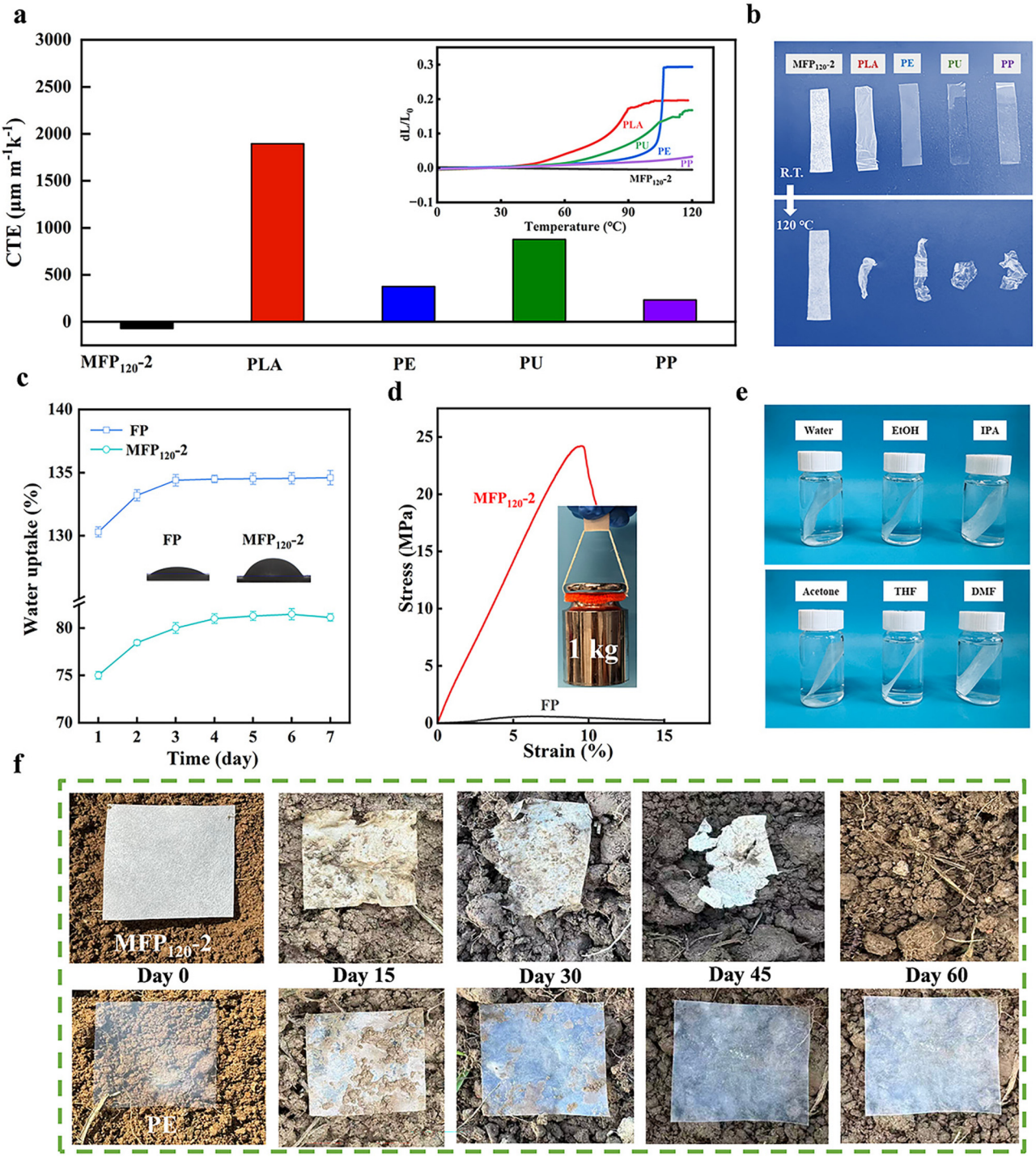

Fig. 5 Thermal stability, water resistance, solvent resistance, and biodegradability of MFP_{120}-2. (a) Comparison of the coefficient of thermal expansion (CTE) and thermal expansion behaviour of MFP_{120}-2 with those of polylactic acid (PLA), polyethylene (PE), polyurethane (PU), and polypropylene (PP). (b) Dimensional stability of MFP_{120}-2 and representative petroleum-based plastics at 27 °C and 120 °C. (c) Water absorption of FP and MFP_{120}-2. (d) Tensile stress–strain curves of FP and MFP_{120}-2 after water immersion for 7 days; the inset shows an MFP_{120}-2 strip supporting a 1000 g load. (e) Structural stability of MFP_{120}-2 after immersion in various organic solvents for 7 days. (f) Photographs illustrating the biodegradation behaviour of MFP_{120}-2 and commercial polyethylene (PE).

fibrous network effectively restricts solvent-induced plasticization and maintains inter-fibre bonding across diverse solvent environments.

Biodegradability is an essential criterion for evaluating the environmental sustainability of cellulose-based bioplastics.[71] To assess end-of-life behavior, the degradation performance of

MFP_{120}-2 was investigated under two representative conditions, namely simulated landfill (winter conditions) and composting environments, and compared with commercial polyethylene (PE) films of identical dimensions (40 mm × 40 mm × 0.1 mm). Under landfill conditions, MFP_{120}-2 undergoes gradual degradation and is completely decomposed within approximately 60 days (Fig. 5f and Fig. S8c). Mass-loss analysis shows an initial slow degradation stage during the first 15 days, followed by accelerated decomposition, likely associated with progressive microbial colonization and structural disintegration of the cellulose network. Under composting conditions, degradation proceeds more rapidly, with complete degradation occurring within 20 days (Fig. S8a and b). In contrast, PE films remained largely intact under both landfill and composting conditions due to their chemically inert and hydrophobic nature. These results demonstrate that MFP_{120}-2 is readily degradable in biologically active environments, highlighting its potential as a sustainable alternative to persistent petroleum-based plastics.

Potential applications of cellulose-based bioplastics

Among common single-use plastic products, drinking straws represent a representative source of plastic waste due to their widespread consumption and limited recyclability. The development of biodegradable cellulose-based alternatives therefore provides an attractive pathway toward reducing disposable plastic usage. However, many commercially available paper straws still suffer from limited mechanical durability and insufficient water stability during use. To demonstrate practical applicability, wet MFP_{120}-2 sheets were rolled onto a glass rod, air-dried, and subsequently detached to fabricate cellulose-based straws, as illustrated in Fig. 6a. During drying, the abundance of hydroxyl groups along cellulose chains promotes inter-fibre hydrogen bonding between cellulose microfibres and *in situ* generated nanofibrils, enabling shape fixation without additional binders or chemical additives.[5] For comparison, straws prepared from FP were fabricated using the same rolling procedure.

To assess the practical applicability of MFP_{120}-2 in straw form, both MFP_{120}-2 and FP paper straws were immersed in water to simulate typical usage conditions. As shown in Fig. 6b, rapid water penetration occurs in the FP straw due to its porous structure, leading to edge delamination and noticeable softening within 30 s. In contrast, the MFP_{120}-2 straw maintains structural integrity after prolonged immersion, exhibiting no apparent delamination even after 4 h in water (Fig. 6c). The improved water stability is consistent with the densified nanofibril–microfibre network formed through LBTH-induced surface reconstruction, which enhances inter-fibre bonding and limits water-induced swelling. To further simulate drinking conditions, vacuum suction generated using a pipette was applied to mimic liquid transport through the straw. Continuous water uptake remains achievable after 4 h of immersion (Fig. S9), indicating preserved functionality during use. Moreover, the MFP_{120}-2 straw retains its tubular geometry after two days of water immersion (Fig. S10). Mechanical flexibility was further evaluated through bending tests in comparison with commercial plastic and paper straws. Commercial paper straws exhibit severe cracking, while plastic straws show irreversible deformation after bending. In contrast, the MFP_{120}-2 straw maintains structural integrity without visible cracking or permanent deformation (Fig. S11), demonstrating balanced flexibility and mechanical robustness. Collectively, these results demonstrate the feasibility of reconstructed cellulose-based bioplastics as durable and water-stable alternatives for single-use straw applications.

A life cycle assessment (LCA) was conducted to evaluate the environmental impact associated with the production of MFP_{120}-2. FP Environmental performance was quantified using the ReCiPe 2016 Midpoint method, covering multiple impact categories including global warming potential (GWP), stratospheric ozone depletion potential (ODP), ionizing radiation potential (IRP), ozone formation (human health, OFHH), fine particulate matter formation potential (PMFP), ozone formation (terrestrial ecosystems, OFTE), terrestrial acidification potential (TAP), freshwater eutrophication potential (FEP), freshwater ecotoxicity potential (FETP), human carcinogenic toxicity potential (HCTP), and land occupation potential (LOP). Contribution analysis (Fig. S12) indicates that FP production dominates land occupation impacts, whereas lithium bromide contributes primarily to terrestrial acidification due to salt production processes. The life cycle inventory is summarized in Table S2 (SI), with FP data obtained from the Ecoinvent v3 database. As FP originates from renewable biomass resources, further reductions in environmental burden may be achievable through sustainable feedstock sourcing.[72] The environmental performance of MFP_{120}-2 straws was further compared with that of commercial PE and PLA straws. From a cradle-to-gate perspective, the GWP of MFP_{120}-2 straws was calculated to be 3.49 kg CO_2-eq per kg product, which is much lower than those of PE (6.97 kg CO_2-eq per kg) and PLA (7.8 kg CO_2-eq per kg) straws (Fig. 6d). Reduced impacts are also observed across several additional categories, including ODP, OFHH, FETP, and HCTP (Fig. S13). Overall, the LCA results indicate that MFP_{120}-2 straws provide a significantly lower environmental footprint relative to representative petroleum-derived and bio-based plastic straws, supporting the potential of solvent-mediated cellulose reconstruction as a sustainable materials manufacturing pathway.

Experimental section

Materials

A medium-speed qualitative filter paper (FP) with a diameter of φ = 11 cm and an ash content of ≤0.15% was used as the pristine cellulose substrate and was purchased from Hangzhou Fuyang Special Paper Co., Ltd, China. Lithium bromide (LiBr, ≥99 wt%) was obtained from Shanghai Aladdin Biochemical Technology Co., Ltd. Commercial PE films were purchased from TOP Daily Chemical (China) Co., Ltd. All chemicals were used as received without further purification. Deionized water was used throughout all experiments.

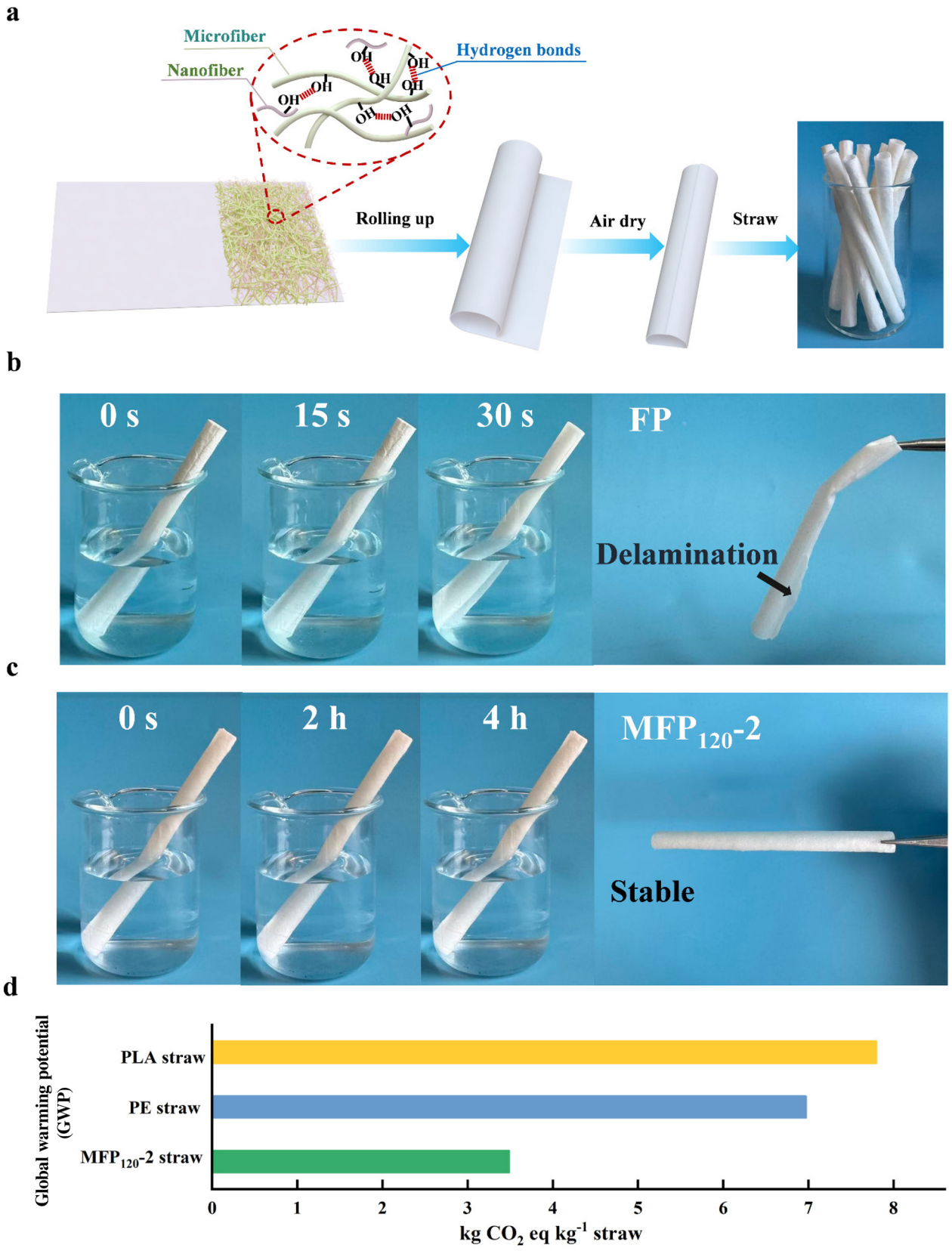

Fig. 6 Demonstration of practical applications of MFP_{120}-2. (a) Schematic illustration of the fabrication process of MFP_{120}-2 paper straws. (b) Water immersion behaviour of an FP paper straw after 30 s. (c) Water immersion behaviour of an MFP_{120}-2 paper straw after 4 h. (d) Comparison of the global warming potential (GWP) of MFP_{120}-2, PE, and PLA straws based on life cycle assessment (LCA).

Preparation of cellulose-based bioplastics

An aqueous lithium bromide solution (61.66 wt%), corresponding to lithium bromide trihydrate (LBTH), was heated to 120 °C and maintained at the target temperature prior to treatment. Pre-dried FP was immersed in the hot LBTH solution for controlled durations of 2 s, 6 s, 10 s, and 20 s; here, the treatment time refers solely to the immersion step and excludes the subsequent washing and hot-pressing processes. After treatment, the samples were immediately removed and thoroughly rinsed multiple times with deionized water (30 mL) several times until the conductivity of the rinse water approached that of fresh deionized water, ensuring effective removal of residual LiBr. The washed, still-wet samples were subsequently hot-pressed at 120 °C under a pressure of 0.1 MPa for 30 s to obtain dry cellulose-based bioplastic sheets. Detailed preparation conditions and sample abbreviations are summarized in Table S1.

Characterization of cellulose-based bioplastics

The chemical structure, morphology, and physicochemical properties of cellulose-based bioplastics were characterized using Fourier transform infrared spectroscopy (FTIR) detections, scanning electron microscopy (SEM), transmission electron microscopy (TEM), X-ray diffraction (XRD), and X-ray photoelectron spectroscopy (XPS). Thermal and dimensional stability were evaluated by thermogravimetric analysis (TGA) and coefficient of thermal expansion (CTE) measurements. Life cycle assessment (LCA) was also conducted. Detailed experimental procedures and characterization conditions are provided in the SI.

Conclusions

In summary, we demonstrate a solvent-mediated strategy for upgrading cellulose paper through surface-confined partial dissolution using a recyclable molten salt hydrate (LBTH). The ultrashort (2 s) treatment induces localized dissociation and reorganization of cellulose chains, generating *in situ* nanofibrils while preserving the original fibrous framework. This controlled structural reconstruction results in a densified nanofibril–microfibre interpenetrating network that simultaneously enhances mechanical strength, wet stability, and dimensional robustness without chemical derivatization or external additives. The reconstructed cellulose-based bioplastic achieves a tensile strength of 69.9 MPa in the dry state and 27.1 MPa under wet conditions, representing substantial improvements over untreated cellulose paper and outperforming most previously reported paper-based plastics. Additionally, the obtained bioplastic exhibits low water uptake, solvent resistance, high thermal stability, and retained biodegradability. Practical fabrication of durable cellulose-based straws further demonstrates the applicability of this bioplastic under realistic service conditions. Life cycle assessment confirms a reduced environmental footprint compared with representative polyethylene and polylactic acid straws. Overall, this work establishes an additive-free and solvent-efficient pathway for transforming conventional cellulose paper into high-performance, biodegradable bioplastics, providing a sustainable alternative to persistent single-use plastics and advancing green manufacturing approaches for biomass-derived materials.

Author contributions

Zhonglei Huang and Meiyan Wu conceived the idea. Ping Wang and Zhonglei Huang contributed equally to this work. Ping Wang carried out the main experiments. Ping Wang and Zhonglei Huang carried out the data organization. Safoora Mirmohamadsaghi assisted with the LCA calculation. Chao Liu and Guang Yu analysed the results. Wang Ping wrote the original manuscript. Haishun Du, Jing Shen and Bin Li supervised the research work. Haishun Du, Jing Shen, Bin Li and Zhonglei Huang revised the manuscript. All authors participated in the interpretation of the data and the production of the final manuscript.

Conflicts of interest

There are no conflicts to declare.

Data availability

Data will be made available on request.

Supplementary information (SI) is available. See DOI: https://doi.org/10.1039/d6gc01239f. The Supplementary Information contains additional experimental characterization methods, sample abbreviations, supporting tensile-property data under dry and wet conditions, SEM morphology, density, thermal stability, oxygen transmission rate, solvent-resistance results, biodegradation behaviour, water-stability and flexibility evaluation of MFP_{120}–2 straws, as well as life-cycle assessment data, life-cycle inventory information, and supplementary references.

Acknowledgements

This work was financially supported by the National Natural Science Foundation of China (No. W2412117, U22A20423 and 22478405), the International Partnership Program of Chinese Academy of Sciences (No. 323GJHZ2023019MI), the Qingdao Science and Technology Demonstration Project (No. 24-1-8-cspz-6-nsh), and the Heilongjiang Natural Science Foundation for Outstanding Young Scholars (No. JQ2023C004). These funding sources supported the work conducted at the authors' affiliated institutions in China. H. Du did not receive financial support from these funding sources.

References

1 T. Xu, H. Du, H. Liu, W. Liu, X. Zhang, C. Si, P. Liu and K. Zhang, *Adv. Mater.*, 2021, **33**, e2101368.
2 K. L. Law, S. Morét-Ferguson, N. A. Maximenko, G. Proskurowski, E. E. Peacock, J. Hafner and C. M. Reddy, *Science*, 2010, **329**, 1185–1188.
3 L. Gu and T. Ozbakkaloglu, *Waste Manage.*, 2016, **51**, 19–42.
4 R. Geyer, J. R. Jambeck and K. L. Law, *Sci. Adv.*, 2017, **3**, e1700782.
5 X. Wang, Z. Pang, C. Chen, Q. Xia, Y. Zhou, S. Jing, R. Wang, U. Ray, W. Gan, C. Li, G. Chen, B. Foster, T. Li and L. Hu, *Adv. Funct. Mater.*, 2020, **30**, 1910417.
6 W. Liu, S. Zhang, K. Liu, H. Yang, Q. Lin, T. Xu, X. Song, H. Du, L. Bai and S. Yao, *J. Cleaner Prod*, 2023, **384**, 13558.
7 C. M. Rochman, A. M. Cook and A. A. Koelmans, *Environ. Toxicol. Chem.*, 2016, **35**, 1617–1626.
8 H. Liu, T. Xu, C. Cai, K. Liu, W. Liu, M. Zhang, H. Du, C. Si and K. Zhang, *Adv. Funct. Mater.*, 2022, **32**, 1.
9 K. Liu, H. Du, T. Zheng, W. Liu, M. Zhang, H. Liu, X. Zhang and C. Si, *Green Chem.*, 2021, **23**, 9723–9746.
10 M Xiao, Y.-J. Liu, E. A. Bayer, A. Kosugi, Q. Cui and Y. Feng, *Green Carbon*, 2024, **2**(1), 57–69.
11 A. Pandey, C. R. Soccol, P. Nigam and V. T. Soccol, *Bioresour. Technol.*, 2000, **74**, 69–80.
12 H. L. Zhu, W. Luo, P. N. Ciesielski, Z. Q. Fang, J. Y. Zhu, G. Henriksson, M. E. Himmel and L. Hu, *Chem. Rev.*, 2016, **116**(16), 9305–9374.
13 P. Sun, S. Wang, Z. Huang, L. Zhang, F. Dong, X. Xu and H. Liu, *Green Chem.*, 2022, **24**, 7519–7530.
14 Y. Zhang, W. Deng, M. Wu, G. Yu, Z. Liu, N. Cheng, H. Du and B. Li, *Green Carbon*, 2024, **2**(2), 231–241.
15 B. Jiang, C. Chen, Z. Liang, S. He, Y. Kuang, J. Song, R. Mi, G. Chen, M. Jiao and L. Hu, *Adv. Funct. Mater.*, 2020, **30**, 1906307.
16 J. Oh, S. Ju and J. M. Koo, *Nat. Rev. Bioeng.*, 2024, **2**, 289–304.
17 D. Negrete-Bolagay and V. H. Guerrero, *Polymers*, 2024, **16**, 2561.
18 X. Li, X. Li, W. Ma and J. Ma, *Carbohydr. Polym.*, 2025, **355**, 123351.
19 J. Su, K. Zhao, Y. Ren, L. Zhao, B. Wei, B. Liu, Y. Zhang, F. Wang, J. Li and Y. Liu, *Angew. Chem., Int. Ed.*, 2022, **61**, e202117538.
20 X. Wang, Y. Liu, X. Liu, X. You and H. J. Zhang, *ACS Appl. Mater. Interfaces*, 2021, **13**, 1367–1376.
21 L. Chen, X. Zhang, T. Qiang, Q. Chen, J. Li and Y. Zhang, *Sustainable Mater. Technol.*, 2025, **45**, e01432.
22 S. Park, K. Lee, G. Bozoklu, W. Cai, S. Nguyen and R. Ruoff', *ACS Nano*, 2008, **2**, 572–578.
23 A. M. Elzaabalawy and A. Shaker, *Chem. Eng. J.*, 2020, **398**, 125403.
24 J. Li, R. Wu, W. J. Wang, K. H. Lim and X. Yang, *Carbohydr. Polym.*, 2023, **321**, 120881.
25 L. Li, X. Qian and J. Shen, *Carbohydr. Polym.*, 2022, **293**, 119728.
26 Z. Lu, H. Zhang, L. Liu, H. Cao, Z. Cheng, H. Liu and X. An, *Ind. Crops Prod.*, 2023, **201**, 116897.
27 D. B. Silva, B. P. M. Ramasini, A. J. M. Comodaro, R. F. Gouveia, N. M. V. Sampaio and J. S. Bernardes, *Chem. Eng. J.*, 2025, **523**, 168186.
28 A. Shankar, A. K. Abdul Malik, R. Narayan and A. Chakrabarty, *Prog. Org. Coat.*, 2023, **182**, 107634.
29 H. Kwak, H. Kim, S.-A. Park, J. Park, D. X. Oh and J. M. Koo, *Adv. Sci.*, 2023, **10**, 2205554.
30 S. Choe, S. You, K. Park, Y. Kim, J. Park, Y. Cho, J. Seo, H. Yang and J. Myung, *Green Chem.*, 2024, **26**, 8230–8241.
31 S. Sen, J. D. Martin and D. S. Argyropoulos, *ACS Sustainable Chem. Eng.*, 2013, **1**, 858–870.
32 Z. Huang, G. Yu, C. Liu, M. Wu, Y. Tang, B. Li and H. Peng, *Carbohydr. Polym.*, 2022, **284**, 119180.
33 X. Li, Z. Chen, X. Guan, H. Jiang, M. Yan, L. Zhang, J. Ma, L. Wang and Z. Wang, *ACS Nano*, 2025, **19**, 20991–21006.
34 M. Lara-Serrano, S. Morales-Delarosa, J. M. Campos-Martin and J. L. G. Fierro, *Green Chem.*, 2020, **22**, 3860–3866.
35 Z. M. Han, D. H. Li, H. B. Yang, Y. X. Zhao, C. H. Yin, K. P. Yang, H. C. Liu, W. B. Sun, Z. C. Ling and Q. F. Guan, *Adv. Funct. Mater.*, 2022, **32**, 2202221.
36 Z. Wei, Z. Gao, J. Sun, J. Guo, Y. Wang, X. Tang, Y. Wang, Z. Xiao, H. Wang and Y. Xie, *Int. J. Biol. Macromol.*, 2025, **321**, 146471.
37 X. Zhou, Y. Fu, L. Chen, R. Wang, X. Wang, Y. Miao, X. Ji, H. Bian and H. Dai, *Carbohydr. Polym.*, 2020, **248**, 116791.
38 D. Xie, R. Zhang, C. Zhang, S. Yang, Z. Xu and Y. Song, *Int. J. Biol. Macromol.*, 2023, **253**, 126959.
39 Y. Chen, H. Y. Yu and Y. Li, *ACS Sustainable Chem. Eng.*, 2020, **8**, 18446–18454.
40 I. F. Kaimin, I. A. Litvinov, V. Y. Khoruna and G. P. Veveris, *Recl. Trav. Chim. Pays-Bas*, 1925, **44**, 451–458.
41 A. Pinkert, K. N. Marsh, S. Pang and M. P. Staiger, *Chem. Rev.*, 2009, **109**, 6712–6728.
42 Z. Huang, C. Liu, X. Feng, M. Wu and B. Li, *Cellulose*, 2020, **27**, 1–14.
43 N. R. Quiroz, A. M. D. Padmanathan, S. H. Mushrif and D. G. Vlachos, *ACS Catal.*, 2019, **9**, 10551–10561.
44 Y. Cao, M. Wu, Y. Gao, Y. Zhang, Z. Zhang, Q. Yang, H. Du, Y. Liu and B. Li, *Small*, 2025, **21**, 2502150.
45 R. Gong, C. Liu, M. Wu, R. Tian, G. Yu, X. Luo, B. Li, F. Peng and Y. Tang, *Green Chem.*, 2024, **26**, 4622–4632.
46 Z. Xueqin, X. Naiyu, W. Huihui, L. Chuanfu and P. Xuejun, *Polymers*, 2018, **10**, 614.
47 X. Yang, L. Yu, B. Zhang, Y. Wang, X. Jia, E. Lizundia, C. Chen, F. Dong, L. Qi and L. Chen, *Nat. Commun.*, 2025, **16**, 6523.
48 J. Liu, C. Wang, C. M. Ewulonu, X. Chen, M. Wu and Y. Huang, *Cellulose*, 2022, **29**, 527–540.
49 A. Poulose, A. Mathew, A. Uthaman, H. M. Lal, J. Parameswaranpillai, A. Mathiazhagan, M. M. Saheed, Y. Grohens, D. Pasquini and D. A. Gopakumar, *Int. J. Biol. Macromol.*, 2024, **255**, 14.
50 L. Qian, D. Lei, X. Duan, S. Zhang, W. Song, C. Hou and R. Tang, *Carbohydr. Polym.*, 2018, **192**, 44–51.

51 P. Micha, S. Grzegorz, B. Tadeusz, G. Agnieszka, S. S. Awomir and K. Izabella, *Polymers*, 2018, **10**, 251.
52 M. J. Staplevan, A. J. Ansari, A. Ahmed and F. I. Hai, *Waste Manage.*, 2024, **185**, 1–9.
53 C. Sun, X. Bu, T. Yang, C. Qiao, X. Ji, F. Tao, L. Gai and L. Liu, *ACS Appl. Polym. Mater.*, 2023, **5**, 5360–5369.
54 H. Huang, F. Ban, Z. Zhang and C. Huang, *Int. J. Biol. Macromol.*, 2025, **307**, 142195.
55 H. Huang, L. Mao, W. Wang, Z. Li and C. Qin, *Int. J. Biol. Macromol.*, 2023, **236**, 123630.
56 Z. Tong, S. Zeng and X. Li, *Carbohydr. Polym.*, 2024, **328**, 122646.
57 C. Wang, S. Wu, N. Zhang, Z. Jiang, X. Hou, L. Huang and T. Deng, *Green Energy Environ.*, 2023, **8**, 1673–1682.
58 S. K. Mohd, Z. Sarani, S. M. Shaiful, G. Sinyee, C. C. Hua, J. S. N. Syed and A. U. Adli, *Int. J. Biol. Macromol.*, 2018, **118**, 181–193.
59 S. Y. Oh, D. I. Yoo, Y. Shin and G. Seo, *Carbohydr. Res.*, 2005, **340**, 417–428.
60 M. Wu, P. Sukyai, D. Lv, F. Zhang, P. Wang, C. Liu and B. Li, *Chem. Eng. J.*, 2020, **392**, 123673.
61 Z. Tong, J. Meng, S. Liu, Y. Liu, S. Zeng, L. Wang, Q. Xia and H. Yu, *Carbohydr. Polym.*, 2021, **272**, 118473.
62 X. Lu and X. Shen, *Carbohydr. Polym.*, 2011, **86**, 239–244.
63 W. Perdoch, Z. Cao, P. Florczak, R. Markiewicz, M. Jarek, K. Olejnik and B. Mazela, *Molecules*, 2022, **27**, 4696.
64 D. H. Li, Z. M. Han, Q. He, K. P. Yang, W. B. Sun, H. C. Liu, Y. X. Zhao, Z. X. Liu, C. N. Zong, H. B. Yang, Q. F. Guan and S. H. Yu, *Adv. Mater.*, 2023, **35**, e2208098.
65 Q. F. Guan, H. B. Yang, Z. M. Han, Z. C. Ling, K. P. Yang, C. H. Yin and S. H. Yu, *Nano Lett.*, 2021, **21**, 8999–9004.
66 V. Agarwal, G. W. Huber, W. C. Conner and S. M. Auerbach, *J. Chem. Phys.*, 2011, **135**, 10B605–10B668.
67 M. Antlauf and O. Andersson, *Macromolecules*, 2022, **55**, 6.
68 K. O. Reddy, C. U. Maheswari, M. S. Dhlamini, B. M. Mothudi, J. Zhang, J. Zhang, R. Nagarajan and A. V. Rajulu, *Carbohydr. Polym.*, 2017, **160**, 203–211.
69 S. Jing, L. Wu, A. P. Siciliano, C. Chen, T. Li and L. Hu, *ACS Nano*, 2023, **17**, 22196–22226.
70 X. Zhang, Y. Cheng, J. You, J. Zhang, C. Yin and J. Zhang, *Nat. Commun.*, 2022, **13**, 1117.
71 R. Yang, G. Xu, W. Tao, Q. Wang and Y. Tang, *Green Carbon*, 2024, **2**, 1–11.
72 S. Wang, A. Cheng, F. Liu, J. Zhang, T. Xia, X. Zeng, W. Fan and Y. Zhang, *Ind. Chem. Mater*, 2023, **1**, 188–206.